四川大学学报（医学版） 2025，56（4）：907－919
J Sichuan Univ（Med Sci）

在线全文

Targeted Delivery of Triptolide Alleviates Diabetic Nephropathy via Inactivation of JAK2-STAT1 Signaling

HUANG Rongshuang[1], *LI Xinrui*[1], *GUO Fan*[1], *LI Yanping*[2], *MA Liang*[1△], *FU Ping*[1]. 1. *Department of Nephrology, Institute of Kidney Diseases, West China Hospital, Sichuan University, Chengdu 610041, China*; 2. *Department of Pharmacy, Institute of Metabolic Diseases and Pharmacotherapy, West China Hospital, Sichuan University, Chengdu 610041, China*

△ Corresponding author, E-mail: liang_m@scu.edu.cn

[Abstract] Objective Inflammation and fibrosis are key features of diabetic nephropathy (DN). Triptolide (TP) exhibits anti-inflammatory and anti-fibrotic properties, though its mechanisms of action in DN remain unclear. CREKA (Cys-Arg-Glu-Lys-Ala) is a pentapeptide that specifically binds to fibronectin (FN), and the CREKA-modified liposome (CREKA-Lip) represents a novel FN-targeted drug delivery system. This study aimed to investigate the role of TP in diabetic db/db mice and determine whether encapsulation within CREKA-Lip enhances therapeutic efficacy while reducing the multi-organ toxicity of TP. **Methods** Eight-week-old diabetic db/db mice received tail vein injections twice weekly with vehicle, free TP, or CREKA-Lip/TP for 10 weeks. Urine and serum parameters were measured, and kidney, heart, liver, and testis tissues were collected for pathological evaluation. Protein-protein interaction networks were constructed using Cytoscape and its plug-ins to identify core targets and elucidate the therapeutic mechanism of TP against DN. Inflammatory, fibrotic, apoptotic, and lipid metabolism markers were evaluated in the kidneys of diabetic mice with DN and in high glucose-treated mouse mesangial cells and podocytes using qPCR, Western blot, immunohistochemistry, and immunofluorescence assays. **Results** TP administration reduced fasting blood glucose levels and glomerular mesangial expansion in diabetic mice. TP significantly suppressed renal inflammation, fibrosis, and apoptosis while enhancing lipid metabolism. Integration of network pharmacology, molecular docking, and transcriptomics revealed that TP ameliorated DN by inhibiting the JAK2-STAT1 signaling pathway. *In vitro*, TP inhibited high glucose-induced phosphorylation of JAK2 and STAT1, reduced collagen production in mesangial cells, decreased apoptosis, and improved lipid metabolism in podocytes. Moreover, CREKA-Lip/TP exhibited superior efficacy compared with free TP, with a more sustained reduction in urine albumin-to-creatinine ratio and greater inhibition of mesangial expansion. Notably, CREKA-Lip/TP treatment did not induce systemic toxicity. **Conclusion** TP improves renal inflammation, fibrosis, apoptosis, and lipid homeostasis, thereby ameliorating DN by inhibiting JAK2-STAT1 activation. Targeted delivery of TP via FN-binding CREKA-Lip enhances therapeutic efficacy while minimizing multi-organ toxicity.

[Key words] Diabetic nephropathy Triptolide STAT1 Polypeptide-liposome Toxicity

靶向递送雷公藤甲素通过抑制JAK2-STAT1信号通路改善糖尿病肾病*

黄蓉双[1]，李鑫睿[1]，郭 帆[1]，李艳萍[2]，马 良[1△]，付 平[1]

1. 四川大学华西医院 肾脏内科/肾脏病研究所（成都 610041）；2. 四川大学华西医院 药剂科/代谢性疾病与药物治疗研究所（成都 610041）

【摘要】 目的 炎症与纤维化是糖尿病肾病（DN）的重要病理特征。雷公藤甲素（TP）具有抗炎抗纤维化作用，但其改善DN的机制尚未明确。CREKA（半胱氨酸-精氨酸-谷氨酸-赖氨酸-丙氨酸）五肽可特异性结合纤维连接蛋白（FN），CREKA修饰脂质体（CREKA-Lip）是一种新型FN靶向给药系统。本研究旨在探究TP对糖尿病db/db小鼠的治疗作用，并评估CREKA-Lip包载能否增强TP疗效并降低其多器官毒性。**方法** 8周龄糖尿病db/db小鼠随机分组，经尾静脉每周2次分别注射溶剂、游离TP或CREKA-Lip/TP，持续10周。检测尿液及血清指标；收集肾脏、心脏、肝脏和睾丸进行病理学评估；基于Cytoscape平台结合插件构建蛋白互作网络并筛选核心靶点，明确TP抗DN的作用靶点；通过qPCR、Western blot、免疫组化及免疫荧光法检测DN糖尿病小鼠肾脏及高糖处理的小鼠系膜细胞、足细胞中炎症、纤维化、凋亡及脂代谢相关指

* 国家自然科学基金（No. 82200973）、四川省自然科学基金项目（No. 2025ZNSFSC1615、No. 2024NSFSC1727）和四川大学华西医院学科卓越发展1·3·5工程项目（No. ZYGD18027）资助

△ 通信作者，E-mail: liang_m@scu.edu.cn

出版日期：2025-07-20

标。**结果** TP给药可降低糖尿病小鼠空腹血糖，减轻肾小球系膜区扩张，显著抑制肾脏炎症反应、纤维化及细胞凋亡，并改善脂代谢紊乱。网络药理学、分子对接及转录组学联合分析表明，TP通过抑制JAK2-STAT1信号通路改善DN。体外实验证实，TP通过抑制高糖诱导的JAK2-STAT1通路磷酸化，减少系膜细胞胶原生成，减轻足细胞凋亡并改善脂代谢。此外，与游离TP相比，CREKA-Lip/TP能更有效且稳定地降低尿白蛋白/肌酐比值(ACR)，对系膜区扩张的抑制作用更强，且给药期间未诱发全身毒性。**结论** TP通过抑制JAK2-STAT1通路活化，改善肾脏炎症、纤维化、凋亡及脂质稳态，从而减轻DN。基于CREKA-Lip的FN靶向递送可增强TP疗效并降低多器官毒性。

【关键词】 糖尿病肾病 雷公藤甲素 STAT1 多肽脂质体 药物毒性

Diabetic nephropathy (DN) is the leading cause of end-stage kidney disease[1]. Pathological features of DN include glomerular basement membrane thickening, mesangial expansion, Kimmelstiel-Wilson lesions, and intramural lipid accumulation in various kidney regions (e.g., glomeruli, tubules)[2]. Among known risk factors, hyperglycemia is the primary driver of DN development. Inflammation and subsequent extracellular matrix (ECM) accumulation are common pathways in DN progression. Proinflammatory cytokines such as interleukin-1 (IL-1), IL-6, and tumor necrosis factors (TNFs) play critical roles in the pathogenesis of DN[3]. Additionally, dyslipidemia is a modifiable contributor to DN[4].

Triptolide (TP), one of the most bioactive components extracted from *Tripterygium wilfordii* Hook.f, exhibits potent immunosuppressive, anti-inflammatory, and anticancer properties[5]. However, TP has poor water solubility and a narrow therapeutic window[6]. Systemic administration of TP may cause severe multi-organ toxicity, prompting the development of alternative drug delivery systems to overcome these limitations. CREKA (Cys-Arg-Glu-Lys-Ala), a pentapeptide that binds specifically to fibronectin (FN)[7], has shown promise in tumor-targeted drug delivery when used to modify liposomes[8-10].

The mechanisms by which TP ameliorates DN have garnered increasing research interest. The Janus kinase–signal transducer and activator of transcription (JAK-STAT) signaling pathway regulates cellular activation, proliferation, and differentiation and is a critical intracellular signaling cascade activated by diabetic stimuli[11]. STAT1, a member of the STAT family, has been found to be activated in DN. Inhibition of STAT1 reduces ECM accumulation[12], epithelial-to-mesenchymal transition (EMT)[13], and high glucose (HG)-induced inflammation and apoptosis[14].

This study employed db/db mice as an *in vivo* DN model to investigate the therapeutic potential of TP in alleviating kidney injury, and used mouse mesangial cells and podocytes *in vitro* to evaluate its protective effects against HG conditions. Additionally, we assessed the therapeutic efficacy and safety of TP delivered via CREKA-modified liposomes (CREKA-Lip), comparing outcomes between CREKA-Lip/TP and free TP treatments in db/db mice.

1 Materials and methods

1.1 Drugs and CREKA-Lip/TP preparation

TP ($C_{20}H_{24}O_6$, purity > 98%) was obtained from Selleck Chemicals (Shanghai, China). Liposomes were prepared according to previously described methods[15]. TP-loaded liposomes were formulated by incorporating TP into the organic lipid solution before solvent evaporation. CREKA-coupled liposomes were synthesized by combining CREKA with maleimide-derivatized PEGylated liposomes (Mal-Lip) at room temperature with overnight stirring.

1.2 Animals

Six-week-old male db/m mice (n = 6) and db/db mice (n = 18) were obtained from GemPharmatech (Jiangsu, China). The mice were maintained on a 12 h/12 h light/dark cycle at (23 ± 1) °C under specific pathogen-free conditions, with unrestricted access to food and drinking water. After a 2-week acclimation period, db/m mice were assigned to the db/m group, and db/db mice were randomly divided into three groups (n = 6 per group). Each group received intravenous administration of vehicle, 50 μg/kg free TP, or CREKA-Lip/TP, respectively, twice weekly for 10 weeks. All animal experiments were approved by the Animal Ethics Committee at West China Hospital of Sichuan University (Approval No. 2020268A, 1 September 2020).

1.3 Serum and urine chemistry analyses

Fasting blood glucose (FBG) levels were measured biweekly from mouse tail veins using the Gold-Accu glucose meter (Sinocare Inc., Changsha, China). Serum creatinine (Scr), alanine aminotransferase (ALT), aspartate

aminotransferase (AST), total cholesterol (TC), triglycerides (TG), and urinary creatinine and albumin (ALB) levels were analyzed using an automatic biochemical analyzer (BS-240, Mindray, Shenzhen, China).

1.4 Histology and pathological analyses

Kidney, liver, heart, and testis tissues were collected, fixed in 10% neutral-buffered formalin, embedded in paraffin, and sectioned at 4 μm. Renal histology was assessed using Periodic acid–Schiff (PAS), Masson, and Sirius Red staining. Liver, heart, and testis sections underwent hematoxylin and eosin (HE) staining. For immunofluorescence analysis, tissues were fixed in optimal cutting temperature compound (Sakura Finetek), stored at −80 °C, and sectioned. Frozen sections were blocked with horse serum for 1 h, followed by overnight incubation with primary antibodies at 4 °C. Sections were washed with PBS and incubated with secondary antibodies. After nuclear staining with DAPI, tissues were visualized.

1.5 qPCR analysis

Total RNA was extracted using the Animal Total RNA Isolation Kit (FOREGENE) and reverse-transcribed into cDNA using the PrimeScript™ RT Reagent Kit (TaKaRa). Real-time PCR was conducted using iTaq™ Universal SYBR® Green (Bio-Rad) on the CFX96 Touch™ Real-Time PCR System (Bio-Rad). The thermal cycling conditions were as follows: 30 s at 95 °C, followed by 39 cycles of 95 °C for 5 s and 57 °C for 30 s, and a melt curve analysis (65-95 °C, 0.5 °C increments, 2-5 s/step). Relative gene expression was calculated using the $2^{-\Delta\Delta Ct}$ method, with β-actin as the endogenous control. All reactions were performed in triplicate. Primers were designed using NCBI Primer-BLAST (further details are provided in Supplementary Table S1 available online at the publisher's website [https://ykxb.scu.edu.cn/]).

1.6 Western blot

Protein samples from renal tissues or cells were separated by sodium dodecyl sulfate-polyacrylamide gel electrophoresis (SDS-PAGE) and transferred to nitrocellulose membranes. After blocking with skimmed milk for 1-2 h, membranes were incubated overnight at 4 °C with the following primary antibodies: anti-FN (BA1772, BOSTER), anti-IL-6 (EM170414), anti-collagen Ⅵ (SD83-03), anti-pJAK2 (ET1607-34), anti-JAK2 (M1501-8), anti-Fatty Acid Synthase (ET1701-91), anti-SREBF-1 (ER1917-19), anti-IL-1β (AF4006), anti-TNF-α (AF7014), anti-collagen Ⅰ (AF7001), anti-pSTAT1 Tyr701 (AF3300), anti-pSTAT1 Ser727 (AF3299), anti-STAT1 (AF6300), anti-PPAR-α (AF5301), and anti-SCD1 (DF13253) from Affinity; anti-BAX (ab32503) and anti-CPA1 (ab128568) from Abcam; anti-Bcl-2 (#3498) from CST; anti-cleaved caspase-3 (6640-2-Ig) from Proteintech; and anti-β-actin (380624) from ZEN-BIOSCIENCE. After three washes with TBST (5 min each), membranes were incubated with horseradish peroxidase-conjugated secondary antibodies (HuaBio) for 1-2 h at room temperature. Following further washing, bands were visualized using an enhanced chemiluminescence system (4A Biotech) and captured on X-ray film. Densitometric quantification was performed using ImageJ software.

1.7 Oil Red O staining

Frozen liver sections were stained with Oil Red O (BaSO Diagnostics Institute, Zhuhai, China) according to standard protocols.

1.8 RNA-sequencing analysis

Total RNA was extracted from kidney tissues of mice from different groups (n = 3 per group). RNA quantity and purity were assessed using the NanoDrop ND-1000 (NanoDrop, DE, USA), and RNA integrity was evaluated with the Bioanalyzer 2100 (Agilent, CA, USA) with a RNA integrity number (RIN) > 7.0, confirmed by denaturing agarose gel electrophoresis. Paired-end sequencing (2 × 150 bp, PE150) was performed on an Illumina NovaSeq™ 6000 (LC-Bio Technology Co., Ltd., Hangzhou, China) following the vendor's recommended protocols for mRNA library construction and sequencing.

1.9 Network pharmacology

Target identification for TP was conducted using TCMSP, Zinc, ChEMBL, BindingDB, Stitch, SuperPred, SwissTargetPrediction, and TTD databases. DN-related targets were identified using the MalaCards database. Protein-protein interaction networks were constructed using Cytoscape with the Bisogenet plug-in. Core targets were determined using Cytoscape with the CytoNAC plug-in. These core targets were subjected to pathway enrichment analysis using the DAVID online tool.

1.10 Molecular docking

The crystal structure of STAT1 was obtained from the

Protein Data Bank, and the 3D structure of TP was downloaded from PubChem. Both structures were converted to pdbqt format using AutoDockTools. Molecular docking and binding affinity calculations were performed using AutoDock Vina. Docking results were visualized using PyMOL software.

1.11 Cell culture

Cells were obtained from the Cell Bank of Type Culture Collection (Chinese Academy of Sciences, Shanghai, China). Mouse mesangial cells were cultured in DMEM (Hyclone), mouse podocytes in RPMI 1640 (Gibco), and human podocytes in McCoy's 5A (Gibco), all supplemented with 10% fetal bovine serum (Gibco) and 1% penicillin-streptomycin. Cells were maintained at 37 °C in a humidified atmosphere with 5% CO_2. Upon reaching 80% confluence, cells were incubated overnight in serum-free medium and then treated for 48 h with normal glucose (NG, 5 mmol/L), HG (30 mmol/L), or TP at low (1.25 ng/mL), medium (2.5 ng/mL), or high doses in 30 mmol/L glucose, depending on experimental requirements.

1.12 Flow cytometry

Apoptosis was analyzed by flow cytometry (CytoFLEX, Beckman Coulter) using an Annexin V-FITC Apoptosis Detection Kit (Sungene Biotech). Cells were washed with cold PBS, treated with 0.5% trypsin, and labeled with Annexin V-FITC and propidium iodide, with excitation at 488 nm.

1.13 Statistical analysis

Data were analyzed using GraphPad Prism 9.0. Continuous variables are expressed as mean ± standard deviation (SD). Comparisons between two groups were conducted using an unpaired Student's *t*-test, while comparisons among three or more groups were performed using one-way analysis of variance (ANOVA), followed by Dunnett's multiple comparisons test for post hoc analysis. $P < 0.05$ was considered statistically significant.

2 Results

2.1 Therapeutic effects of TP against DN

Body weight and food intake were monitored biweekly following administration. The results indicated that neither parameter was affected by TP treatment (further details are provided in Supplementary Figure S1 available online at the publisher's website [https://ykxb.scu.edu.cn/]). However, TP significantly reduced the FBG level in db/db mice, from (18.8 ± 6.9) mmol/L to (10.3 ± 5.9) mmol/L (Table 1). PAS (Figure 1A), Masson (Figure 1B), and Sirius Red (Figure 1C) staining revealed mesangial expansion and collagen accumulation in the kidneys of db/db mice, while TP treatment substantially ameliorated these changes (Figure 1D). Urinary ALB-to-creatinine ratio (ACR) was measured biweekly; however, no significant reduction was observed in the TP group (Figure 1E). Serum TC, TG, ALB, and Scr levels were assessed after 10 weeks of administration. TP demonstrated therapeutic effects on dyslipidemia, although Scr levels remained consistent across groups (further details are provided in Supplementary Figure S2 available online at the publisher's website [https://ykxb.scu.edu.cn/]).

2.2 TP ameliorated renal inflammation, fibrosis, and apoptosis in DN

To evaluate the therapeutic effect of TP on DN, we analyzed kidney inflammation, fibrosis, and apoptosis, which are common features in the progression of DN. Western blotting revealed that renal proinflammatory cytokines IL-6, IL-1β, and TNF-α were elevated in the db/db

Table 1 Fasting blood glucose during TP administration

Group	*c*(FBG)/(mmol/L)				
	0 week	2 weeks	4 weeks	8 weeks	10 weeks
db/m	4.70 ± 1.15**	4.28 ± 0.71***	4.00 ± 0.24***	3.47 ± 0.55***	3.65 ± 0.78****
db/db	—	16.38 ± 4.78	17.27 ± 3.10	18.13 ± 3.60	18.77 ± 6.93
Free TP	14.29 ± 4.50	11.85 ± 5.72	18.5 ± 6.80	12.02 ± 8.42	10.33 ± 5.87*
CREKA-Lip/TP	—	10.6 ± 3.38	13.88 ± 5.45	5.97 ± 3.11***	6.24 ± 0.87***

$n = 6$ independent samples. $^{*}P < 0.05$, $^{**}P < 0.01$, $^{***}P < 0.001$, $^{****}P < 0.000\,1$, vs. db/db group.

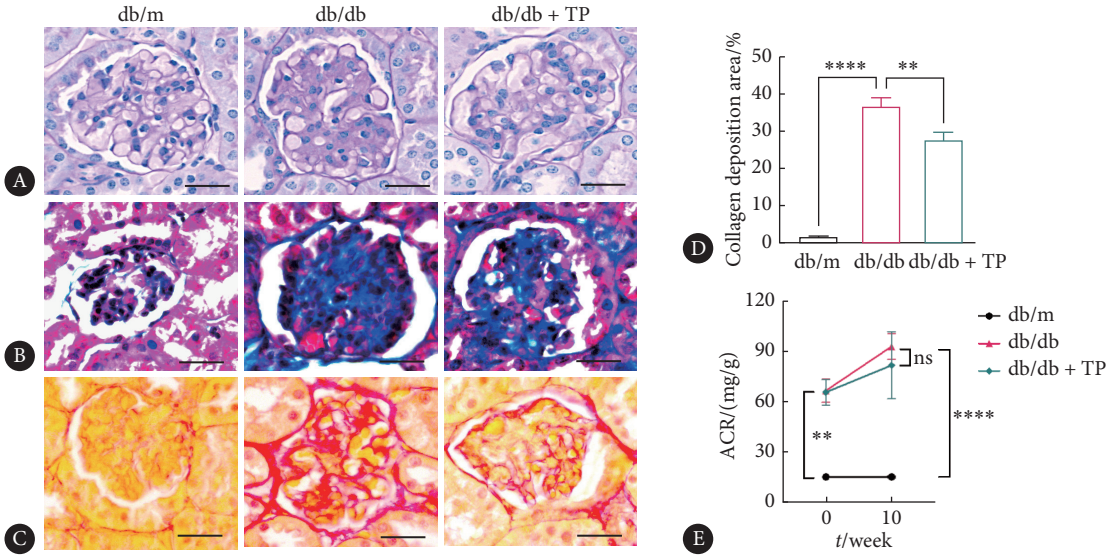

Fig 1　Triptolide improved pathological damage of diabetic nephropathy

Histological damage was assessed using Periodic acid–Schiff (PAS) (A), Masson (B), and Sirius Red (C) staining. D, Comparison of collagen deposition areas among different groups. E, Urine albumin-to-creatinine ratio (ACR) at the conclusion of TP administration. The scale bar represents 10 μm. n = 6 independent samples. ns: P > 0.05; $^{**}P$ < 0.01, $^{****}P$ < 0.000 1.

group and were subsequently suppressed by TP administration (Figure 2A). TP also reduced the expression of collagen Ⅰ and Ⅵ, as well as FN (Figure 2B). Regarding apoptosis, TP increased the protein level of Bcl2 while reducing the expression of BAX and cleaved caspase-3, the active form of caspase-3 (Figure 2C).

2.3　TP improved kidney lipid metabolism in DN

Lipid droplet deposition in glomeruli was assessed

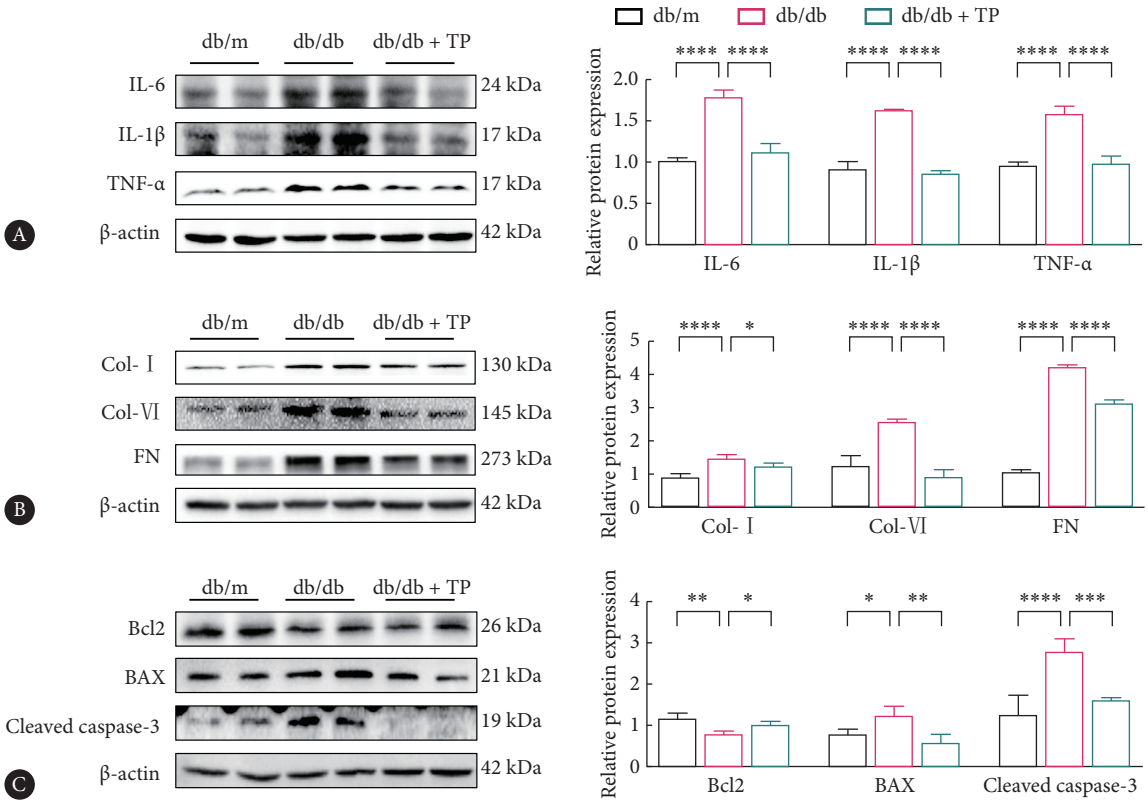

Fig 2　Triptolide ameliorated kidney inflammation, fibrosis, and apoptosis in db/db mice

A, Protein levels of IL-6, IL-1β, and TNF-α were detected by Western blot. B, Expression of fibrotic proteins (collagen Ⅰ, Ⅵ, and fibronectin). C, Expression of apoptosis-related proteins (Bcl2, BAX, and cleaved caspase-3). n = 4 independent samples. $^{*}P$ < 0.05, $^{**}P$ < 0.01, $^{***}P$ < 0.001, $^{****}P$ < 0.000 1.

through Oil Red O staining (Figure 3A). While lipid droplets were present in the kidneys of the db/m group, they were localized to tubules rather than glomeruli. However, significant lipid droplets were observed in the glomeruli Nevertheless, noticeable lipid droplets could be seen in glomeruli of db/db mice, with fewer droplets in the TP group. Analysis of genes associated with lipid synthesis and β-oxidation was conducted. qPCR analysis demonstrated that TP decreased the mRNA expression of lipogenic genes *Srebf-1*, *Fasn*, and *Scd-1* (Figure 3B-3D). Conversely, TP significantly increased the mRNA expression of *Ppar-α* (Figure 3E) and *Cpt-1* (Figure 3F), genes involved in fatty acid oxidation.

2.4 TP ameliorated DN by inhibiting JAK2-STAT1 pathway

We further investigated the mechanism of TP in treating DN through network pharmacology. Analysis identified 121 and 87 proteins as targets of TP and DN, respectively. Topology analysis of the protein-protein interaction networks revealed 5 164 proteins in the TP-predicted target network and 2 277 in the DN-predicted network. The intersection yielded 1 442 proteins common to both TP and DN. Based on association strength, 327 core targets were ultimately identified (Figure 4A). Core target enrichment analysis suggested that TP might ameliorate DN by binding to STAT1 and inhibiting the JAK2-STAT1 pathway (further details are provided in Supplementary Figure S3 available online at the publisher's website [https://ykxb.scu.edu.cn/]). AutoDock predicted the docking pose of TP with STAT1 (Figure 4B), showing a binding energy of −5.66 kcal/mol. Compared with the STAT1/DNA complex (PDB entry: 10.2210/pdb1BF5/pdb, Figure 4C), we hypothesized that TP occupied the DNA-binding site of STAT1, thereby preventing the expression of downstream inflammatory and fibrotic genes.

Next, we validated the *in vivo* inhibitory effect of TP on

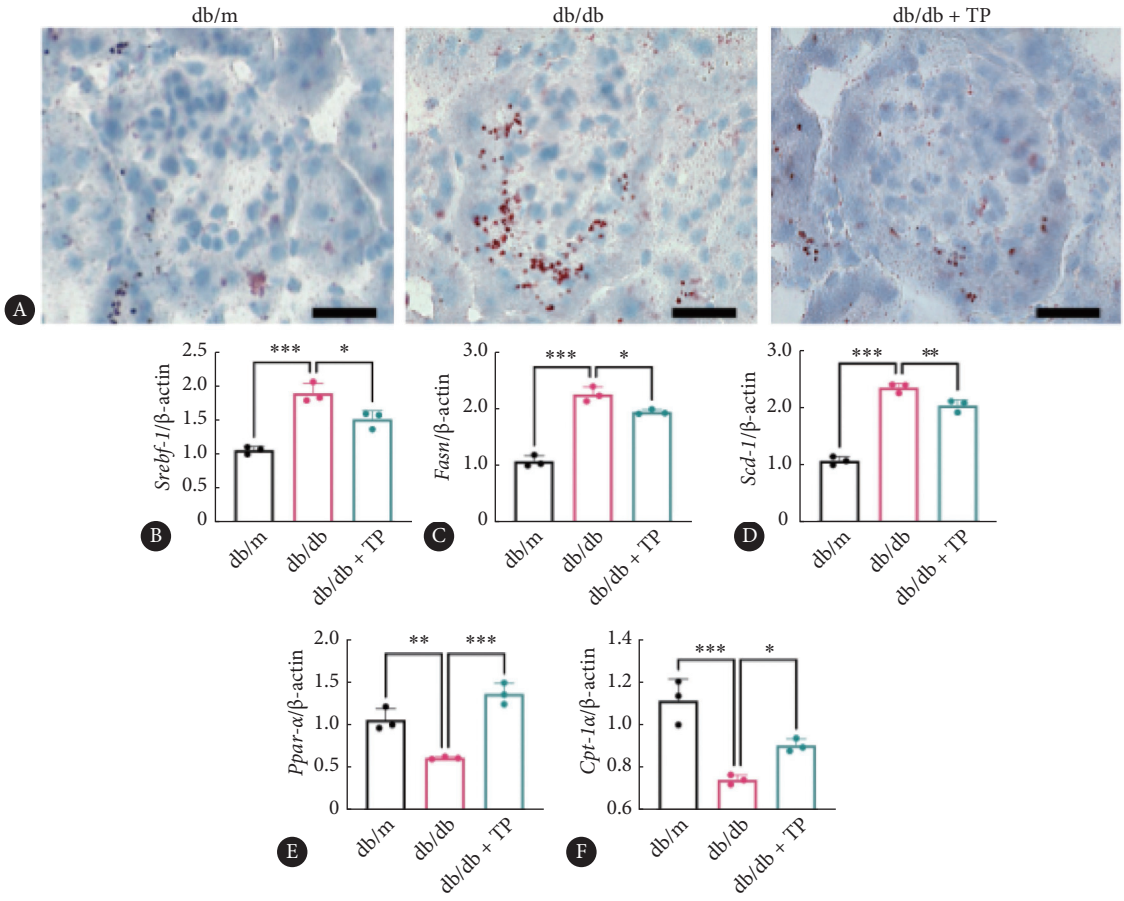

Fig 3 Triptolide improved lipid metabolism in the kidneys of db/db mice

A, Oil Red O staining of kidney sections from each group (the scale bar represents 10 μm). B-F, mRNA levels of genes related to lipid synthesis (*Srebf-1*, *Fasn*, and *Scd-1*) and β-oxidation (*Ppar-α* and *Cpt-1α*), assessed by qPCR. $n = 3$ independent samples. $^{*}P < 0.05$, $^{**}P < 0.01$, $^{***}P < 0.001$, $^{****}P < 0.000\,1$.

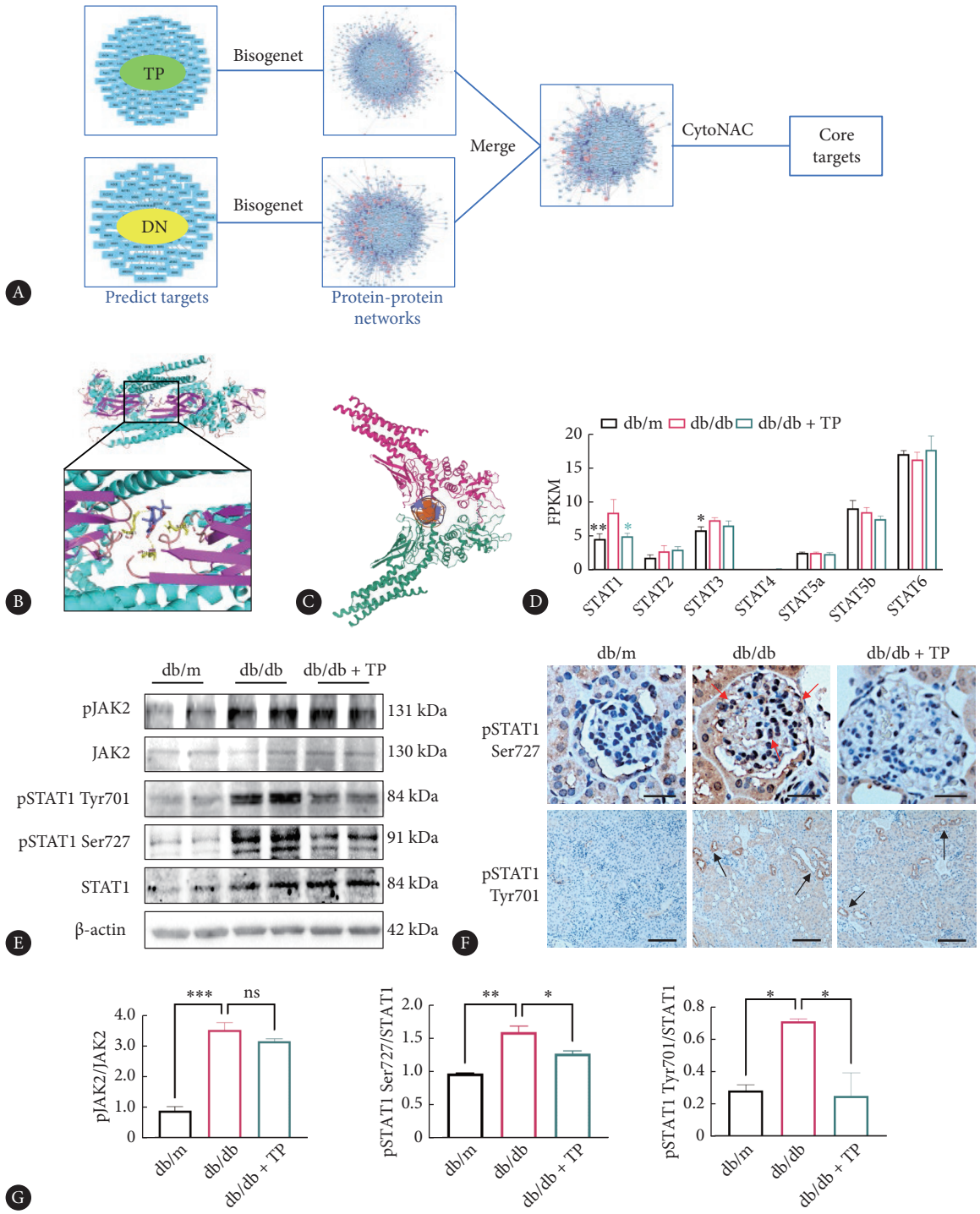

Fig 4 Triptolide reversed the activation of JAK2-STAT1 in the kidneys of db/db mice

A, Schematic of the process used to identify core targets. B, Molecular docking model of TP with STAT1. C, Docking of the STAT1 dimer with DNA. D, RNA-sequencing results showing expression levels of STAT1-6. E, Western blot detection of JAK2-STAT1 pathway proteins. F, Immunohistochemical analysis of pSTAT1 (Ser727 and Tyr701), positive in the glomerulus was indicated by a red arrow, and positive in the renal tubule was indicated by a black arrow. The scale bar represents 10 μm. G, Relative expression of pJAK2 and pSTAT1 (Ser727 and Tyr701), $n = 3$ or 4 independent samples. ns: $P > 0.05$; $^{*}P < 0.05$, $^{**}P < 0.01$, $^{***}P < 0.001$.

the JAK2-STAT1 pathway. RNA sequencing revealed that STAT1 showed the most significant variation among STAT family members (Figure 4D). STAT1 contains two phosphorylation sites: Tyr701 and Ser727. Western blot demonstrated that TP significantly inhibited the phosphorylation of JAK2-STAT1 pathway in the kidneys of db/db mice (Figure 4E, 4G). Immunohistochemistry of pSTAT1 indicated that the positive staining area of pSTAT1

Ser727 in glomeruli was greater in the db/db group than in the db/m group, while TP treatment reduced this staining (Figure 4F). pSTAT1 Tyr701 was detected exclusively in tubular epithelial cells.

2.5 TP suppressed collagen production in HG-stimulated mesangial cells

To explore the potential mechanism of TP against DN, mouse mesangial cells were cultured under HG conditions. The TP concentration gradient was determined using a CCK8 assay (further details are provided in Supplementary Figure S4 available online at the publisher's website [https://ykxb.scu.edu.cn/]). As shown in Figure 5, HG-treated mesangial cells exhibited activated JAK2-STAT1 phosphorylation and increased collagen production (Col-Ⅰ, Col-Ⅵ, and FN). Notably, TP treatment significantly inhibited JAK2-STAT1 activation and reduced collagen production in a concentration-dependent manner (Figure 5).

2.6 TP mitigated apoptosis and improved lipid metabolism in HG-induced podocytes

Given that podocyte injury contributes to the progression of DN, we investigated the effects of TP on HG-treated podocytes. Initial results confirmed that HG activated phosphorylation of JAK2 and STAT1, which was suppressed by TP in a dose-dependent manner (Figure 6A). Lipogenic proteins (SREBF-1, FASN, and SCD-1) showed increased expression in the HG group compared with the NG group and were dose-dependently inhibited by TP. Conversely, β-oxidation–related proteins (PPAR-α and CPT-1α) were downregulated in HG-stimulated podocytes but were restored by TP treatment (Figure 6B). Apoptosis was assessed by flow cytometry and Western blot. Flow cytometry revealed that apoptotic cells comprised 6.87% in the NG group, increasing to 25.03% in the HG group (Figure 6C). The TP 2.5 ng/mL and 5 ng/mL groups showed reduced apoptotic indices (12.60% and 10.23%, respectively). Western blot showed that HG upregulated BAX and cleaved caspase-3, which TP inhibited in a dose-dependent manner, while TP restored the HG-reduced Bcl2 expression (Figure 6D).

2.7 CREKA-Lip/TP exhibited a better therapeutic effect against DN

Similar to free TP, CREKA-Lip/TP did not affect body weight or food intake in db/db mice (further details are

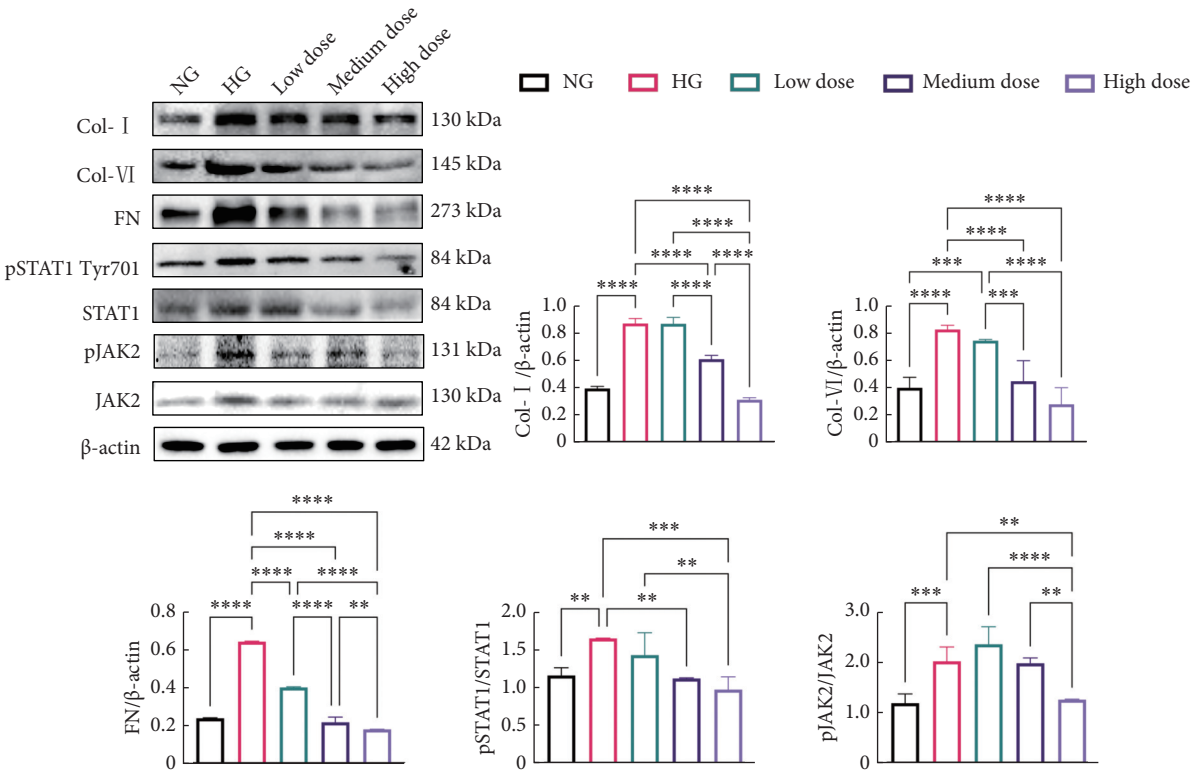

Fig 5 Triptolide suppressed JAK2-STAT1 activation and reduced collagen production in high glucose-induced mesangial cells

NG, normal glucose; HG, high glucose. Expression levels of collagen Ⅰ, collagen Ⅵ, fibronectin, JAK2, and STAT1 proteins were assessed by Western blot, with quantitative densitometric analysis. $n = 4$ biologically independent samples. $^{**}P < 0.05$, $^{***}P < 0.001$, $^{****}P < 0.000\,1$.

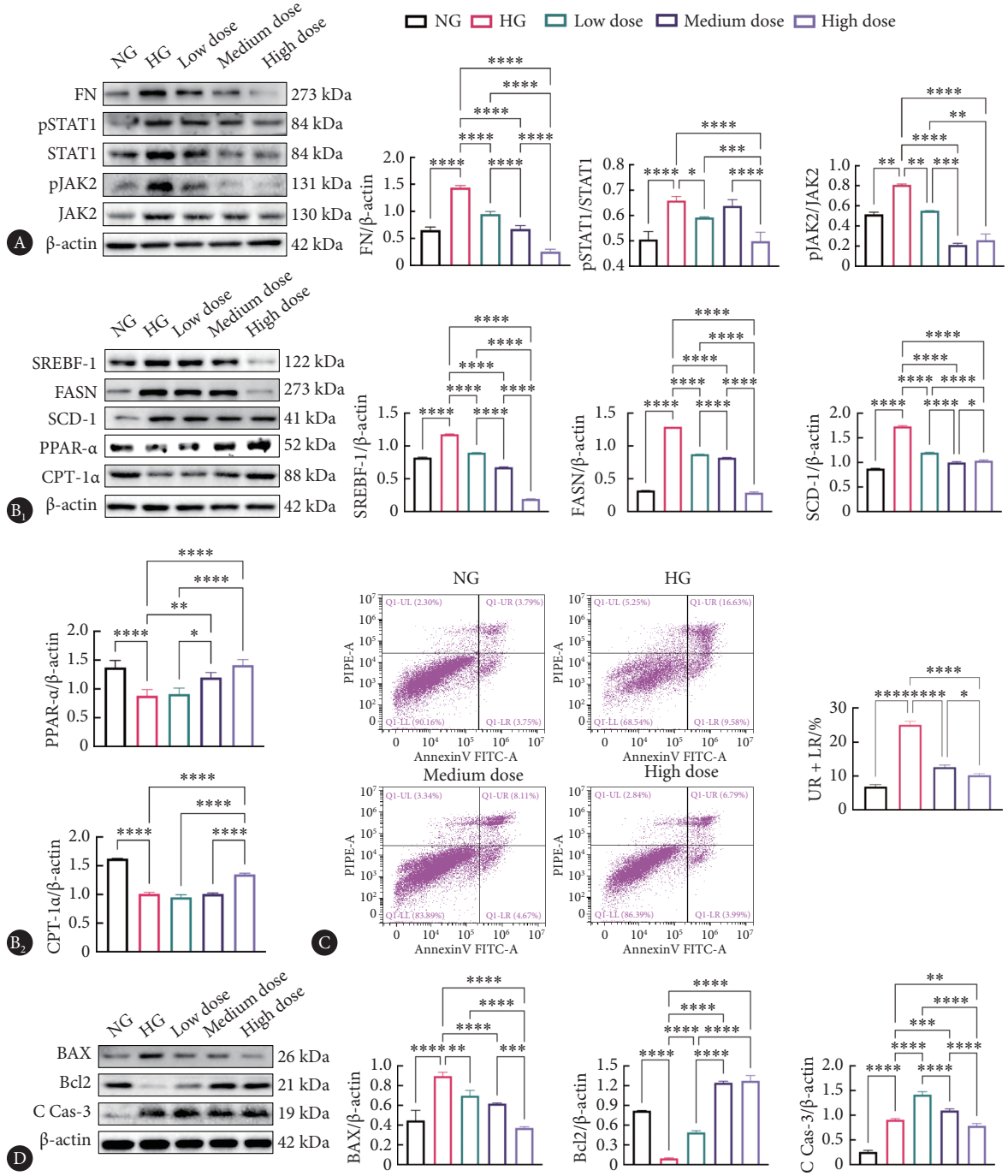

Fig 6　Triptolide ameliorated apoptosis and fatty acid metabolism in high glucose-induced podocytes

NG, normal glucose; HG, high glucose; C Cas-3: cleaved caspase-3. A, TP inhibited JAK2-STAT1 activation and fibronectin expression induced by high glucose. B_1 and B_2, Representative Western blot of proteins involved in lipid synthesis and β-oxidation. C, Apoptotic cells detected by flow cytometry. D, Western blot analysis of apoptosis-related proteins. $n = 3$ or 4 biologically independent samples. $^{*}P < 0.05$, $^{**}P < 0.01$, $^{***}P < 0.001$, $^{****}P < 0.000\,1$.

provided in Supplementary Figure S1 available online at the publisher's website [https://ykxb.scu.edu.cn/]). Serum levels of TC, TG, ALB, and Scr were comparable between the free TP and CREKA-Lip/TP groups (further details are provided in Supplementary Figure S2 available online at the publisher's website [https://ykxb.scu.edu.cn/]). However, CREKA-Lip/TP exhibited superior hypoglycemic effects compared with free TP (Table 1). While the ACR in the free TP group fluctuated significantly, CREKA-Lip/TP reduced ACR more effectively and consistently (Figure 7A). CREKA-Lip/TP also substantially reversed mesangial expansion and collagen accumulation in the kidneys of

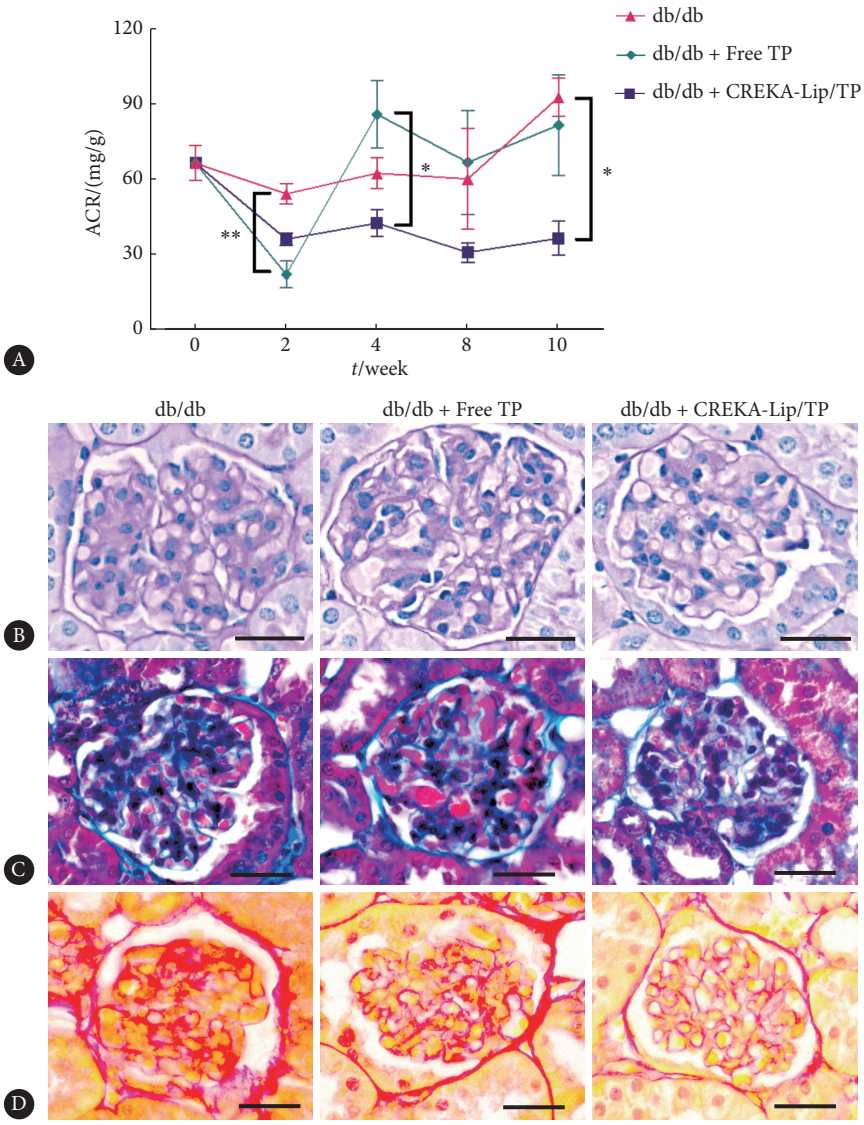

Fig 7 CREKA-Lip/TP showed superior therapeutic effect against diabetic nephropathy compared to free triptolide

A, Urine albumin-to-creatinine ratio (ACR) during treatment. B-D, Histological changes shown by PAS staining (B), Masson staining (C), and Sirius Red staining (D). The scale bar represents 10 μm. $n = 6$ independent samples. $^{*}P < 0.05$, $^{**}P < 0.01$.

db/db mice (Figure 7B-7D).

Western blot (Figure 2B) and qPCR (Figure 8C) analyses revealed significantly elevated FN expression in the kidneys of db/db mice compared with db/m mice. Immunohistochemistry staining of FN (Figure 8A) showed that increased expression was primarily localized to glomeruli. Immunofluorescence staining further revealed co-localization of FN and pSTAT1 Ser727 (Figure 8B), suggesting that CREKA-Lip/TP targets DN glomeruli via FN binding. Furthermore, CREKA-Lip/TP exhibited equivalent or superior effects in anti-fibrotic (Figure 8C), anti-inflammatory (Figure 8D), and anti-apoptotic (Figure 8E) responses compared to free TP.

2.8 CREKA-Lip/TP did not cause systemic toxicity

HE staining of liver, heart, and testis sections, along with serum ALT and AST levels, showed that CREKA-Lip/TP did not induce systemic toxicity (Figure 9A-9C). Notably, CREKA-Lip/TP ameliorated fatty liver. HE staining showed large fat vacuoles in liver sections from db/db mice, which were reduced in volume and number following free TP treatment. The CREKA-Lip/TP group exhibited even fewer and smaller vacuoles, along with more distinct lobular and sinusoidal structures. Although daily administration of TP at doses ⩾ 50 μg/kg induced testicular toxicity, reducing administration frequency and encapsulating TP in CREKA-Lip significantly mitigated this

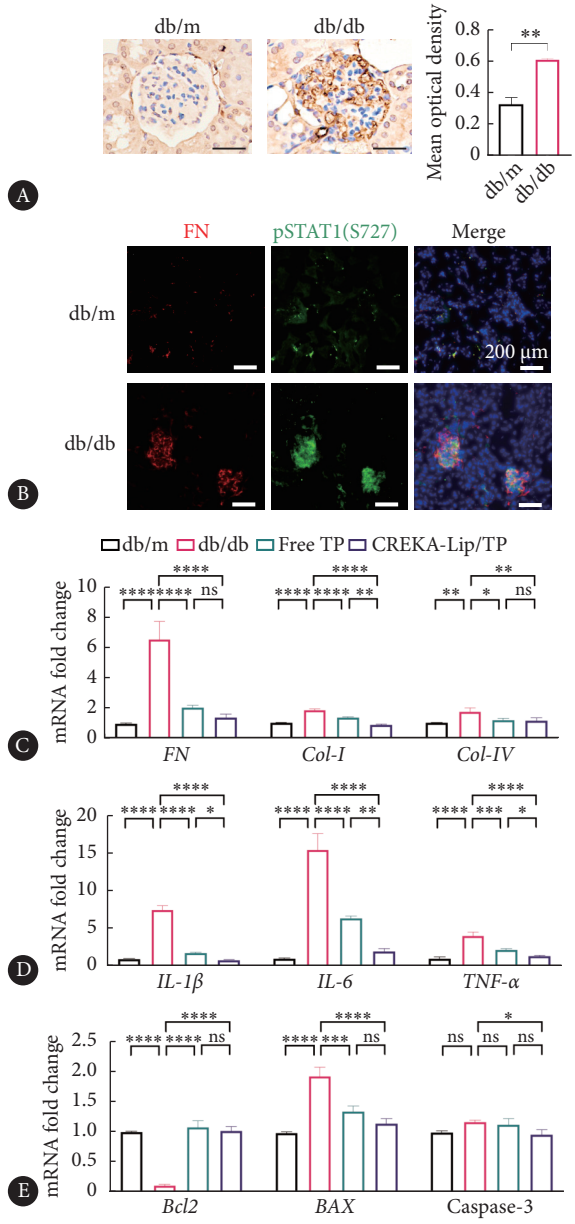

Fig 8 CREKA-Lip/TP inhibited fibrosis, inflammation and apoptosis in the kidneys of db/db mice

A, Immunohistochemistry showing predominant FN expression in glomeruli, The scale bar represents 10 μm. B, Immunofluorescence staining demonstrating co-localization of FN and pSTAT1 Ser727. C, mRNA levels of fibrosis-related genes (*FN*, *Col-Ⅰ*, and *Col-Ⅳ*), D, inflammation-related genes (*IL-1β*, *IL-6*, and *TNF-α*), E, and apoptosis-related genes (*Bcl2*, *BAX*, and caspase-3) were determined by qPCR. $n = 3$ independent samples. ns: $P > 0.05$; $^{*}P < 0.05$, $^{**}P < 0.01$, $^{***}P < 0.001$, $^{****}P < 0.000\,1$.

adverse effect (Figure 9C).

3 Discussion

This study conducted a comprehensive evaluation of the therapeutic effect of TP on DN through *in vivo* and *in vitro* experiments. Network pharmacology and molecular docking results indicated that TP inhibits the JAK-STAT1 pathway, a finding subsequently confirmed by transcriptomic and Western blot. Under diabetic conditions, HG induced abnormalities in mesangial cells and podocytes. *In vitro*, TP inhibited HG-induced collagen production in mesangial cells. In HG-treated podocytes, TP reduced apoptosis and enhanced lipid metabolism. In db/db mice, TP administration decreased mesangial expansion and lipid droplet deposition in glomeruli, supporting the *in vitro* findings. To address TP's systemic toxicity, FN-targeted polypeptide-liposomes (CREKA-Lip) were employed for TP delivery. CREKA-Lip/TP demonstrated a superior and sustained reduction of ACR and greater inhibition of mesangial expansion than free TP, without inducing systemic toxicity.

In DN, JAK-STAT signaling pathway is activated in response to various stimuli, including HG, advanced glycogen end-products, ROS, and angiotensin Ⅱ[16-17]. JAK/STAT1 activation promotes inflammation, oxidative stress, apoptosis of podocytes and tubular cells, and FN synthesis in mesangial cells, thereby accelerating DN progression[12, 14]. STAT1 also modulates lipid metabolism in adipocytes[18]. The present results demonstrate that TP-mediated STAT1 inhibition reduces renal inflammation, fibrosis, apoptosis, and lipid dysregulation in HG-treated podocytes.

Although TP is recognized for its anti-fibrotic and anti-inflammatory properties, its specific mechanisms of action in DN remain unclear. Prior studies have documented TP's ability to inhibit EMT through multiple pathways[19-20] and its protective effects on mesangial cells and podocytes[21-25]. However, no prior research has identified a common target of TP in both cell types. Based on *in vivo* evidence, this study suggests that TP ameliorates DN by protecting mesangial cells and podocytes from HG-induced damage through inhibition of the JAK2-STAT1 pathway.

Beyond its therapeutic effect on DN, TP exhibited potent hypoglycemic activity, an effect rarely reported previously. This action may be attributed to improvements in non-alcoholic fatty liver disease[26]. Recent research has shown that a comparable dose of TP effectively treats non-alcoholic fatty liver disease[27]. Given that intensive glycemic control provides renal benefits[28], the metabolic regulatory

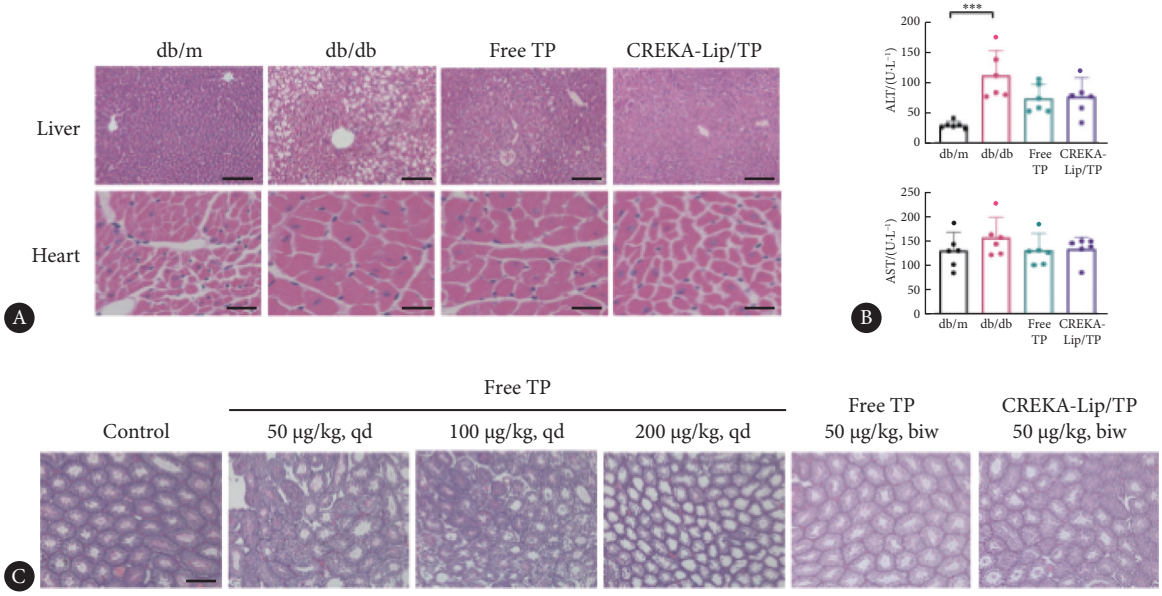

Fig 9 CREKA-Lip/TP did not induce systemic damage

A, HE staining of liver and heart tissues. B, Serum levels of liver transaminases (ALT and AST). C, HE staining of testis under different TP doses and administration frequencies. The scale bar represents 10 μm. $n = 6$ independent samples. *** $P < 0.001$.

effects of TP warrant further investigation.

TP toxicity can be reduced with intermittent low-dose administration, though this often compromises therapeutic effectiveness, particularly in controlling urinary ALB excretion. To enhance efficacy while minimizing toxicity, various TP delivery systems have been developed, including ligand conjugates (e.g., sugars, peptides, antibodies)[29] and nanovehicles (e.g., folate/glutathione-modified nanoparticles and lysozyme conjugates)[30-33]. While mesangial-targeted PEG-coated TRX-20 liposomes[34] and renal tubule-targeted HDL nanoparticles[35] show promise, none have been applied in DN treatment. In this study, both mesangial cells and podocytes exhibited elevated FN expression under HG conditions, prompting the use of FN-targeted CREKA-Lip for TP delivery. CREKA-Lip/TP demonstrated greater efficacy than free TP in treating DN without inducing systemic toxicity, consistent with its anti-fibrotic efficacy in ureteral obstruction models[15]. These findings support CREKA-Lip as a promising platform for delivering hydrophobic drugs in fibrotic kidney diseases.

In summary, TP attenuates renal inflammation, fibrosis, apoptosis, and lipid dysregulation in DN by inhibiting the JAK2-STAT1 pathway. FN-targeted delivery via CREKA-Lip enhances therapeutic efficacy while reducing multi-organ toxicity.

* * *

Author Contribution HUANG Ronghuang is responsible for conceptualization, data curation, and writing--review and editing. LI Xinrui is responsible for formal analysis, investigation, and writing--original draft. GUO Fan is responsible for formal analysis, methodology, and validation. LI Yanping is responsible for methodology and resources. MA Liang is responsible for conceptualization, project administration, and supervision. FU Ping is responsible for funding acquisition and resources. All authors consented to the submission of the article to the Journal. All authors approved the final version to be published and agreed to take responsibility for all aspects of the work.

Declaration of Conflicting Interests FU Ping is a member of the Editorial Board of the journal. All processes involved in the editing and reviewing of this article were carried out in strict compliance with the journal's policies and there was no inappropriate personal involvement by the author. Other than this, all authors declare no competing interests.

References

[1] KALANTAR-ZADEH K, JAFAR T H, NITSCH D, *et al*. Chronic kidney disease. Lancet, 2021, 398: 786-802. doi: 10.1016/S0140-6736(21)00519-5.

[2] UBARA Y, SAWA N, YAMANOUCHI M, *et al*. New interpretation of diabetic nephropathy or diabetic kidney disease from kidney biopsy: review article. Clin Exp Nephrol, 2025, 29: 875-887. doi: 10.1007/s10157-025-02661-4.

[3] RAYEGO-MATEOS S, RODRIGUES-DIEZ R R, FERNANDEZ-FERNANDEZ B, *et al*. Targeting inflammation to treat diabetic kidney disease: the road to 2030. Kidney Int, 2023, 103: 282-296. doi: 10.1016/j.kint.2022.10.030.

[4] BRENNAN E, KANTHARIDIS P, COOPER M E, *et al*. Pro-resolving lipid mediators: regulators of inflammation, metabolism and kidney function. Nat Rev Nephrol, 2021, 17: 725-739. doi: 10.1038/s41581-021-00454-y.

[5] SONG J, HE G N, DAI L. A comprehensive review on celastrol, triptolide and triptonide: Insights on their pharmacological activity, toxicity,

combination therapy, new dosage form and novel drug delivery routes. Biomed Pharmacother, 2023, 162: 114705. doi: 10.1016/j.biopha.2023.114705.
[6] LIANG D, MAI H, RUAN F, *et al*. The efficacy of triptolide in preventing diabetic kidney diseases: a systematic review and Meta-analysis. Front Pharmacol, 2021, 12: 728758. doi: 10.3389/fphar.2021.728758.
[7] ZHOU Z, QUTAISH M, HAN Z, *et al*. MRI detection of breast cancer micrometastases with a fibronectin-targeting contrast agent. Nat Commun, 2015, 6: 7984. doi: 10.1038/ncomms8984.
[8] OKUR A C, ERKOC P, KIZILEL S. Targeting cancer cells via tumor-homing peptide CREKA functional PEG nanoparticles. Colloids Surf B Biointerfaces, 2016, 147: 191-200. doi: 10.1016/j.colsurfb.2016.08.005.
[9] WANG C, WANG X, ZHONG T, *et al*. The antitumor activity of tumor-homing peptide-modified thermosensitive liposomes containing doxorubicin on MCF-7/ADR: *in vitro* and *in vivo*. Int J Nanomedicine, 2015, 10: 2229-2248. doi: 10.2147/IJN.S79840.
[10] JIANG K, SONG X, YANG L, *et al*. Enhanced antitumor and anti-metastasis efficacy against aggressive breast cancer with a fibronectin-targeting liposomal doxorubicin. J Control Release, 2018, 271: 21-30. doi: 10.1016/j.jconrel.2017.12.026.
[11] HU X, LI J, FU M, *et al*. The JAK/STAT signaling pathway: from bench to clinic. Signal Transduct Target Ther, 2021, 6: 402. doi: 10.1038/s41392-021-00791-1.
[12] HE H, WANG H, CHEN X, *et al*. Treatment for type 2 diabetes and diabetic nephropathy by targeting Smad3 signaling. Int J Biol Sci, 2024, 20: 200-217. doi: 10.7150/ijbs.87820.
[13] HUANG F, WANG Q, GUO F, *et al*. FoxO1-mediated inhibition of STAT1 alleviates tubulointerstitial fibrosis and tubule apoptosis in diabetic kidney disease. EBioMedicine, 2019, 48: 491-504. doi: 10.1016/j.ebiom.2019.09.002.
[14] XING Y W, LIU K Z. Azithromycin inhibited oxidative stress and apoptosis of high glucose-induced podocytes by inhibiting STAT1 pathway. Drug Dev Res, 2021, 82: 990-998. doi: 10.1002/ddr.21801.
[15] LI R, LI Y, ZHANG J, *et al*. Targeted delivery of celastrol to renal interstitial myofibroblasts using fibronectin-binding liposomes attenuates renal fibrosis and reduces systemic toxicity. J Control Release, 2020, 320: 32-44. doi: 10.1016/j.jconrel.2020.01.017.
[16] BANES-BERCELI A K, SHAW S, MA G, *et al*. Effect of simvastatin on high glucose- and angiotensin Ⅱ-induced activation of the JAK/STAT pathway in mesangial cells. Am J Physiol Ren Physiol, 2006, 291: F116-21. doi: 10.1152/ajprenal.00502.2005.
[17] HUANG J S, LEE Y H, CHUANG L Y, *et al*. Cinnamaldehyde and nitric oxide attenuate advanced glycation end products-induced the JAK/STAT signaling in human renal tubular cells. J Cell Biochem, 2015, 116: 1028-1038. doi: 10.1002/jcb.25058.
[18] YOU W, LIU S, LI J, *et al*. GADD45A regulates subcutaneous fat deposition and lipid metabolism by interacting with Stat1. BMC Biol, 2023, 21: 212. doi: 10.1186/s12915-023-01713-z.
[19] LI Y, HU Q, LI C, *et al*. PTEN-induced partial epithelial-mesenchymal transition drives diabetic kidney disease. J Clin Invest, 2019, 129: 1129-1151. doi: 10.1172/JCI121987.
[20] REN L, WAN R, CHEN Z, *et al*. Triptolide alleviates podocyte epithelial-mesenchymal transition via kindlin-2 and EMT-related TGF-β/Smad signaling pathway in diabetic kidney disease. Appl Biochem Biotechnol, 2022, 194: 1000-1012. doi: 10.1007/s12010-021-03661-2.
[21] WANG H Q, WU H X, SHI W Q, *et al*. Triptolide attenuates renal slit diagram to tight junction transition in diabetic kidney disease by regulating Nrf2-ferroptosis pathway. Am J Chin Med, 2024, 52: 2161-2185. doi: 10.1142/S0192415X24500836.
[22] HAN F, WANG S, CHANG Y, *et al*. Triptolide prevents extracellular matrix accumulation in experimental diabetic kidney disease by targeting microRNA-137/Notch1 pathway. J Cell Physiol, 2018, 233: 2225-2237. doi: 10.1002/jcp.26092.
[23] MA R, LIU L, LIU X, *et al*. Triptolide markedly attenuates albuminuria and podocyte injury in an animal model of diabetic nephropathy. Exp Ther Med, 2013, 6: 649-656. doi: 10.3892/etm.2013.1226.
[24] LV C, CHENG T, ZHANG B, *et al*. Triptolide protects against podocyte injury in diabetic nephropathy by activating the Nrf2/HO-1 pathway and inhibiting the NLRP3 inflammasome pathway. Ren Fail, 2023, 45: 2165103. doi: 10.1080/0886022X.2023.2165103.
[25] GAO J, LIANG Z, ZHAO F, *et al*. Triptolide inhibits oxidative stress and inflammation via the microRNA-155-5p/brain-derived neurotrophic factor to reduce podocyte injury in mice with diabetic nephropathy. Bioengineered, 2022, 13: 12275-12288. doi: 10.1080/21655979.2022.2067293.
[26] NASR P, FREDRIKSON M, EKSTEDT M, *et al*. The amount of liver fat predicts mortality and development of type 2 diabetes in non-alcoholic fatty liver disease. Liver Int, 2020, 40: 1069-1078. doi: 10.1111/liv.14414.
[27] HUANG R, GUO F, LI Y, *et al*. Activation of AMPK by triptolide alleviates nonalcoholic fatty liver disease by improving hepatic lipid metabolism, inflammation and fibrosis. Phytomedicine, 2021, 92: 153739. doi: 10.1016/j.phymed.2021.153739.
[28] GALINDO R J, BECK R W, SCIOSCIA M F, *et al*. Glycemic monitoring and management in advanced chronic kidney disease. Endocr Rev, 2020, 41: 756-774. doi: 10.1210/endrev/bnaa017.
[29] XU H, LIU B. Triptolide-targeted delivery methods. Eur J Med Chem, 2019, 164: 342-351. doi: 10.1016/j.ejmech.2018.12.058.
[30] YANG M, MENG J, HAN L, *et al*. Pharmacokinetic study of triptolide nanocarrier in transdermal drug delivery system-combination of experiment and mathematical modeling. Molecules, 2023, 28: 553. doi: 10.3390/molecules28020553.
[31] CHEN D, XU J, LV S, *et al*. Enzyme-activatable kidney-targeted dendrimer-drug conjugate for efficient childhood nephrotic syndrome therapy. Theranostics, 2024, 14: 6991-7006. doi: 10.7150/thno.101606.
[32] GUO Q, GENG K, WAN J, *et al*. Lysozyme-targeted liposomes for enhanced tubular targeting in the treatment of acute kidney injury. Acta Biomater, 2025, 192: 394-408. doi: 10.1016/j.actbio.2024.12.026.
[33] YUAN Z X, HE X K, WU X J, *et al*. Peptide fragments of human serum albumin as novel renal targeting carriers. Int J Pharm, 2014, 460: 196-204. doi: 10.1016/j.ijpharm.2013.10.041.
[34] YUAN Z, JIA L, LIM L Y, *et al*. Renal-targeted delivery of triptolide by entrapment in pegylated TRX-20-modified liposomes. Int J Nanomedicine, 2017, 12: 5673-5686. doi: 10.2147/IJN.S141095.
[35] HE S, LI X, HE Y, *et al*. High-density lipoprotein nanoparticles spontaneously target to damaged renal tubules and alleviate renal fibrosis by remodeling the fibrotic niches. Nat Commun, 2025, 16: 1061. doi: 10.1038/s41467-025-56223-z.

（2025－04－10收稿，2025－06－09修回）

编辑　汤　洁